Inverse Problems and Imaging
Volume 1, No. 3, 2007, 457–479

Web site: http://www.aimSciences.org

A NEW EXACT INVERSION METHOD FOR EXPONENTIAL RADON TRANSFORM USING THE HARMONIC ANALYSIS OF THE EUCLIDEAN MOTION GROUP

Can Evren Yarman and Birsen Yazici

Rensselaer Polytechnic Institute
Department of Electrical, Computer and System Engineering
110 8th Street, Troy, NY 12180, USA

(Communicated by Margaret Cheney)

Abstract. This paper presents a new method for the exponential Radon transform inversion based on the harmonic analysis of the Euclidean motion group of the plane. The proposed inversion method is based on the observation that the exponential Radon transform can be modified to obtain a new transform, defined as the modified exponential Radon transform, that can be expressed as a convolution on the Euclidean motion group. The convolution representation of the modified exponential Radon transform is block diagonalized in the Euclidean motion group Fourier domain. Further analysis of the block diagonal representation provides a class of relationships between the spherical harmonic decompositions of the Fourier transforms of the function and its exponential Radon transform. These relationships and the block diagonalization lead to three new reconstruction algorithms. The proposed algorithms are implemented using the fast implementation of the Euclidean motion group Fourier transform and their performances are demonstrated in numerical simulations. Our study shows that convolution representation and harmonic analysis over groups motivates novel solutions for the inversion of the exponential Radon transform.

1. Introduction

For a uniform attenuation coefficient $\mu \in \mathbb{C}$, the exponential Radon transform of a compactly supported real valued function f over $\mathbb{R}^2$ is defined as

$$\mathcal{T}_\mu f(\boldsymbol{\theta}, t) = \int_{\mathbb{R}^2} f(\boldsymbol{x})\delta(\boldsymbol{x}\cdot\boldsymbol{\theta} - t)\mathrm{e}^{\mu \boldsymbol{x}\cdot\boldsymbol{\theta}^\perp} d\boldsymbol{x}, \tag{1}$$

where $t \in \mathbb{R}$, $\boldsymbol{\theta} = (\cos\theta, \sin\theta)^T$ is a unit vector on S^1 and $\boldsymbol{\theta}^\perp = (-\sin\theta, \cos\theta)^T$ with $\theta \in [0, 2\pi)$.

The exponential Radon transform constitutes a mathematical model for imaging modalities such as x-ray tomography ($\mu = 0$), single photon emission tomography (SPECT) ($\mu \in \mathbb{R}$) [1], and optical polarization tomography of stress tensor field ($\mu \in \mathrm{i}\mathbb{R}$) [2].

A number of different methods have been proposed for the inversion of the exponential Radon transform. One of them is the filtered backprojection type inversion method which was first introduced by Tretiak et al. in [3]. This method is based

2000 *Mathematics Subject Classification:* Primary: 44A12, 44A35, 94A08; Secondary: 65R10, 92C55.

Key words and phrases: Exponential Radon transform, convolution representation, Radon transform, ray transform, harmonic analysis, Euclidean motion group.

on the adjoint of the exponential Radon transform and a filter derived from a convolution property of the adjoint operator.

In [4], Hawkins et al. used the filtered back projection method introduced in [3] together with the spherical harmonic decomposition and expressed the circular harmonic decomposition of the function f in terms of the circular harmonic decomposition of its projections $\mathcal{T}_\mu f$. In [5] and [6], Metz et al. and Kuchment et al. introduced alternative filtered backprojection type inversion methods.

In [7], Bellini et al. developed an alternative inversion method by reducing the inversion of the exponential Radon transform to finding the solution of an ordinary differential equation. This approach leads to a relationship between the circular harmonic decomposition of the Fourier transform of f and the circular harmonic decomposition of the Fourier transform of $\mathcal{T}_\mu f$. An alternative method of inversion based on the circular harmonic decomposition of the Fourier transform of f and $\mathcal{T}_\mu f$ was derived by Tretiak et al. [3] and Inouye et al. [8] using two different approaches. In [5], Metz et. al. suggested a weighted linear summation of positive and negative frequencies of the circular harmonic decomposition of the Fourier transform of projections for reconstruction. It was shown that different choices of weight functions provide reconstruction formulas proposed in [7, 3, 8].

In this paper, we present an alternative inversion method for the exponential Radon transform based on the harmonic analysis of the Euclidean motion group. Our approach starts with the modification of the exponential Radon transform:

$$\mathcal{T}'_\mu f(\boldsymbol{\vartheta}, r_1, r_2) = \mathcal{T}_\mu f(\boldsymbol{\vartheta}, -r_1)\mathrm{e}^{\mu r_2}, \qquad \boldsymbol{\vartheta} = (\cos\theta, -\sin\theta)^T,\ r_1, r_2 \in \mathbb{R}. \tag{2}$$

We refer to the resulting transform $\mathcal{T}'_\mu$ as the *modified exponential Radon transform*. Next, we show that the modified exponential Radon transform can be expressed as a convolution of a known kernel and the function $f(-R_\phi \boldsymbol{x})$, $\phi \in [0, 2\pi)$, over the Euclidean motion group ($M(2)$) of the plane (Equation (24)), where R_ϕ is the rotation matrix of ϕ degrees in the clockwise direction.

We next use the Euclidean motion group Fourier transform to block diagonalize the modified exponential Radon transform and develop deconvolution type inversion methods for $\mathcal{T}'_\mu f$. We derived two new reconstruction methods based on the block diagonal representation of the modified exponential Radon transform. Analysis of the block diagonal representation shows that for every column of the matrix representation of the $M(2)$-Fourier transform of $\mathcal{T}'_\mu f$, we obtain the circular harmonic decomposition of the Fourier transform of f as a weighted linear combination of the circular harmonic decomposition of the Fourier transform of $\mathcal{T}_\mu f$. We derived a third reconstruction method from this class of relationships for each column index of the matrix representation of $\mathcal{T}'_\mu f$. However, the former two reconstruction methods are not based on a single weighted relationship, but they combine all the relationships provided by the matrix representations of the $M(2)$-Fourier transform.

All three reconstruction methods are numerically implemented using the fast implementation of the $M(2)$-Fourier transform [9] and their performance is compared with the filtered backprojection algorithm in [3].

Our approach shows that convolution formulation of the exponential Radon transform based on its invariances and the use of harmonic analysis elucidate new and novel solutions for the exponential Radon transform inversion. Furthermore our approach has the following advantages: (i) convolution representation can be extended to angle-dependent and half-scan exponential Radon transform (Appendix C), as well as other integral transforms of emission and transmission tomography;

(ii) while our present work is in deterministic setting, the proposed deconvolution type inversion method provides an effective framework to incorporate a priori object and noise information and can be formulated in either statistical or deterministic setting [10]; (iii) the sampling issues are naturally addressed by the numerical implementation of the fast Fourier transform algorithms over the Euclidean motion group [9].

The rest of the paper is organized as follows: In Section 2, the Euclidean motion group, its Fourier transform and properties are introduced. The convolution representation of the modified exponential Radon transform, its block diagonalization, and the reconstruction formulas are presented in Section 3. In Section 4, derivation of a class of relationships from the block diagonal representation is presented. Section 5 describes the reconstruction algorithms based on the fast implementation of the Fourier transform of the Euclidean motion group, discuss their numerical performance and present numerical simulations. Section 6 summarizes our results and conclusion. The paper concludes with three appendices. The first one provides a review of the basic concepts from the group representation theory and a review of the Fourier transform over groups. The second one provides the extension of the concept of distribution and its Fourier transform to the Euclidean motion group. The third one provides convolution representation of the angle dependent exponential Radon transform and the half-scan problem.

2. Harmonic analysis of the Euclidean motion group

2.1. Euclidean Motion Group. The rigid motions of $\mathbb{R}^2$ are made up of translations and rotations. Translations form the group $\mathbb{R}^2$ with group operation being the vector addition. Any rotation of $\mathbb{R}^2$ can be represented as an 2×2 unitary matrix parameterized by $\theta \in [0, 2\pi)$, R_θ, i.e.

$$R_\theta = \begin{bmatrix} \cos\theta & -\sin\theta \\ \sin\theta & \cos\theta \end{bmatrix}. \tag{3}$$

Rotations of $\mathbb{R}^2$ form the group $SO(2)$ with matrix product being the group operation.

The rigid motions of $\mathbb{R}^2$ form the group called the *Euclidean motion group* of the plane, denoted by $M(2)$. The elements of the group are 3×3 matrices of the form

$$(R_\theta, \boldsymbol{r}) = \begin{bmatrix} R_\theta & \boldsymbol{r} \\ \mathbf{0}^T & 1 \end{bmatrix}, \quad R_\theta \in SO(2),\ \boldsymbol{r} \in \mathbb{R}^2, \tag{4}$$

parameterized by a rotation component θ and a translation component $\boldsymbol{r}$. The group operation of $M(2)$ is the usual matrix multiplications and inverse of an element is obtained by matrix inversion as $(R_\theta, \boldsymbol{r})^{-1} = (R_\theta^{-1}, -R_\theta^{-1}\boldsymbol{r})$. This defines $M(2)$ as the semidirect product of the additive group of $\mathbb{R}^2$ and $SO(2)$.Therefore, $M(2)$ has a natural action on $\mathbb{R}^2$ given by $\boldsymbol{x} \longrightarrow g\boldsymbol{x} = R_\theta \boldsymbol{x} + \boldsymbol{r}$, for a $g = (R_\theta, \boldsymbol{r}) \in M(2)$.

2.2. Fourier Transform over the Euclidean Motion Group. We provide a brief review of the Fourier transforms over groups and definitions of the basic concepts in Appendix A. For a detailed treatment of the topic, we refer the reader to [11] and [12].

The irreducible unitary representations, $U^{(\lambda)}(g)$, of $M(2)$ over $L^2(S^1)$ is given by the following linear operators:

$$(U^{(\lambda)}(g)F)(\boldsymbol{s}) = \mathrm{e}^{-\mathrm{i}\lambda(\boldsymbol{r}\cdot\boldsymbol{s})} F(R_\theta^{-1}\boldsymbol{s}), \quad F \in L^2(S^1), \tag{5}$$

where $g = (R_\theta, \boldsymbol{r}) \in M(2)$, $\boldsymbol{s}$ is a point on the unit circle S^1, $(\,\cdot\,)$ is the standard inner product over $\mathbb{R}^2$, and λ is a nonnegative real number [12].

Let $f \in L^2(M(2))$, then its *Fourier transform* over the Euclidean motion group is defined as [11, 12]

$$\mathcal{F}_{M(2)}(f)(\lambda) = \hat{f}(\lambda) = \int_{M(2)} f(g) U^{(\lambda)}(g^{-1})\, d(g), \tag{6}$$

where $g = (R_\theta, \boldsymbol{r})$, $d(g) = d\boldsymbol{r}d(\theta) = \frac{1}{2\pi} d\boldsymbol{r}d\theta$ is the normalized Haar measure on $M(2)$ with $d(\theta)$ is the normalized Haar measure on $SO(2)$ [1], and the *inverse Fourier transform* is given by

$$\mathcal{F}^{-1}_{M(2)}(\hat{f})(g) = f(g) = \frac{1}{(2\pi)^2} \int_0^\infty \text{Trace}\left(\hat{f}(\lambda) U^{(\lambda)}(g)\right) \lambda d\lambda. \tag{7}$$

For the rest of the paper, the Fourier transform over the Euclidean motion group will be called $M(2)$-*Fourier transform*, for short.

The $M(2)$-Fourier coefficients are operator valued functions that can be expressed in terms of matrices given an orthonormal basis over $L^2(S^1)$.

The *circular harmonics* $\{S_m\}$ form an orthonormal basis for $L^2(S^1)$ [13]. Then the matrix elements $u^{(\lambda)}_{mn}(g)$ of $U^{(\lambda)}(g)$ are given by [12]

$$u^{(\lambda)}_{mn}(g) = (S_m, U^{(\lambda)}(g) S_n) = \int_{S^1} \overline{S_m(\boldsymbol{\omega})} \mathrm{e}^{-\mathrm{i}\lambda \boldsymbol{r}\cdot\boldsymbol{\omega}} S_n(R_\theta^{-1}\boldsymbol{\omega}) d(\boldsymbol{\omega}). \tag{8}$$

If the complex exponentials $\{\mathrm{e}^{\mathrm{i}n\psi}\}$, $n \in \mathbb{Z}$ are chosen as an orthonormal basis for $L^2(S^1)$, the matrix elements for the unitary representation $U^{(\lambda)}(g)$ of $M(2)$ become [12]:

$$u^{(\lambda)}_{mn}(g) = (\mathrm{e}^{\mathrm{i}m\psi}, U^{(\lambda)}(g)\mathrm{e}^{\mathrm{i}n\psi}) = \frac{1}{2\pi} \int_0^{2\pi} \mathrm{e}^{-\mathrm{i}m\psi} \mathrm{e}^{-\mathrm{i}(r_1\lambda\cos\psi + r_2\lambda\sin\psi)} \mathrm{e}^{\mathrm{i}n(\psi-\theta)} d\psi, \quad \forall m, n \in \mathbb{Z}. \tag{9}$$

Alternatively, $u^{(\lambda)}_{mn}(g)$ can be expressed as

$$u^{(\lambda)}_{mn}(g) = \mathrm{i}^{n-m} \mathrm{e}^{-\mathrm{i}[n\theta + (m-n)\phi]} J_{n-m}(\lambda r), \tag{10}$$

where $\boldsymbol{r} = r(\cos\phi, \sin\phi)$ and $J_n(r)$ is the n^{th} order Bessel function,

The matrix elements of $U^{(\lambda)}(g)$ satisfy the following properties:

$$u^{(\lambda)}_{mn}(g^{-1}) = \overline{u^{(\lambda)}_{nm}(g)}, \tag{11}$$

$$u^{(\lambda)}_{mn}(g_1 g_2) = \sum_k u^{(\lambda)}_{mk}(g_1) u^{(\lambda)}_{kn}(g_2). \tag{12}$$

Furthermore, the matrix elements $u^{(\lambda)}_{mn}(g)$ of $U^\lambda(g)$ form a complete orthonormal system in $L^2(M(2))$.

Given the matrix elements of the unitary representations, the $M(2)$-Fourier and inverse $M(2)$-Fourier transforms can be expressed as follows [11]:

$$\mathcal{F}_{M(2)}(f)_{mn}(\lambda) = \hat{f}_{mn}(\lambda) = \int_{M(2)} f(g) u^{(\lambda)}_{mn}(g^{-1}) d(g), \tag{13}$$

$$\mathcal{F}^{-1}_{M(2)}(\hat{f}_{mn})(g) = f(g) = \frac{1}{(2\pi)^2} \int_0^\infty \sum_{m,n} \hat{f}_{mn}(\lambda) u^{(\lambda)}_{nm}(g) \lambda d\lambda. \tag{14}$$

Using (13) and (9), the $M(2)$-Fourier matrix elements can be expressed as

$$\hat{f}_{mn}(\lambda) = \frac{1}{(2\pi)^2}\int_0^{2\pi}\left(\left[\int_0^{2\pi}\left[\int_{\mathbb{R}^2} f(g)\mathrm{e}^{\mathrm{i}(r_1\lambda\cos\psi + r_2\lambda\sin\psi)}dr_1dr_2\right]\mathrm{e}^{\mathrm{i}m\theta}d\theta\right]\mathrm{e}^{-\mathrm{i}m\psi}\right)\mathrm{e}^{\mathrm{i}n\psi}d\psi. \tag{15}$$

Equation (15) shows that given $\{\mathrm{e}^{\mathrm{i}n\psi}\}_{n\in\mathbb{Z}}$ as the orthonormal basis for $L^2(S^1)$, computing the $M(2)$-Fourier transform of f is equivalent to computing four consecutive standard Fourier transforms. First two Fourier transforms are due to the integration over $\mathbb{R}^2$. The last two Fourier transforms are due to the integrations over $\theta \in [0, 2\pi)$ and $\phi \in [0, 2\pi)$.

For the rest of the paper, the orthonormal basis $\{S_m\}$ of $L^2(S^1)$ is assumed to be the complex exponential $\{\mathrm{e}^{\mathrm{i}m\phi}\}$.

Here, the properties of the $M(2)$-Fourier transform that are relevant to rest of our discussion are presented:

1. *Adjoint property:* Let $f \in L^2(M(2))$, then

$$\widehat{f^*}_{mn}(\lambda) = \hat{f}^{\dagger}_{mn} = \overline{\hat{f}_{nm}(\lambda)}, \tag{16}$$

   where $f^*(g) = \overline{f(g^{-1})}$.
2. *Convolution property:* Let $f_1,\ f_2 \in L^2(M(2))$, and let $g = (R_\theta, \boldsymbol{r})$ and $h = (R_\phi, \boldsymbol{x})$. Convolution over $M(2)$ is defined by

$$(f_1 *_{M(2)} f_2)(g) = \int_{M(2)} f_1(h) f_2(h^{-1}g)d(h). \tag{17}$$

   Then

$$\mathcal{F}_{M(2)}(f_1 *_{M(2)} f_2)(\lambda) = \mathcal{F}_{M(2)}(f_2)(\lambda)\cdot\mathcal{F}_{M(2)}(f_1)(\lambda), \tag{18}$$

   or equivalently,

$$\mathcal{F}_{M(2)}(f_1 *_{M(2)} f_2)_{mn}(\lambda) = \sum_q \widehat{f}_{2mq}(\lambda)\ \widehat{f}_{1qn}(\lambda). \tag{19}$$

3. *$M(2)$-Fourier transform of $SO(2)$ invariant functions:* Let $f(g) = f(\boldsymbol{r}) \in L^2(\mathbb{R}^2)$. Let $\widetilde{f}(\boldsymbol{\varepsilon})$ denote the standard Fourier transform of f, i.e.

$$\widetilde{f}(\boldsymbol{\varepsilon}) = \int_{\mathbb{R}^2} f(\boldsymbol{r})\mathrm{e}^{-\mathrm{i}\boldsymbol{r}\cdot\boldsymbol{\varepsilon}}\,d\boldsymbol{r}. \tag{20}$$

   The circular harmonic decomposition $\widetilde{f}_n(\lambda)$ of $\widetilde{f}(\boldsymbol{\varepsilon})$ is defined by

$$\widetilde{f}_n(\lambda) = \int_{S^1} \widetilde{f}(\lambda\boldsymbol{\omega})S_n(\boldsymbol{\omega})\,d(\boldsymbol{\omega}), \tag{21}$$

   where $\boldsymbol{\varepsilon} = \lambda\boldsymbol{\omega}$ is the polar representation. Then

$$\hat{f}_{mn}(\lambda) = \delta_{0m}\widetilde{f}_n(-\lambda), \qquad \lambda \geq 0, \quad m, n \in \mathbb{Z} \tag{22}$$

   where δ_{0m} is the Kronecker delta function, 1 if $m = 0$, else 0. Hence, the $M(2)$-Fourier transform over $\mathbb{R}^2$ is equivalent to performing a standard Fourier transform followed by spherical harmonic decomposition. Similarly, the inverse $M(2)$-Fourier transform $\hat{f}$ of $f \in L^2(\mathbb{R}^2)$, is obtained by reversing the order and the operations performed in the $M(2)$-Fourier transform.

   Conversely, any function $f \in L^2(\mathbb{R}^2)$ can be treated as a $SO(2)$ invariant function over $M(2)$, by $f(g) = f(R_\theta, \boldsymbol{r}) = f(\boldsymbol{r})$. This extension is not only well-defined, but also treats f as an $L^2(M(2))$ function, since $SO(2)$ is a

compact subgroup of $M(2)$ and the measure on $\mathbb{R}^2$ is invariant under the action of $M(2)$.

4. *Band-limitedness* Let $\hat{f}_{mn}(\lambda)$ be the $M(2)$-Fourier transform of a function $f \in L^2(M(2))$. Then f is said to be band-limited if there exist $m_0, n_0 \in \mathbb{Z}^+$, and $\lambda_0 > 0$ such that $\hat{f}_{mn}(\lambda) = 0$ for $|m| > m_0$, $|n| > n_0$ and $\lambda > \lambda_0$.
   - If f is band-limited so is f^*.
   - If f_1 and f_2 are two band-limited functions, then $f_1 *_{M(2)} f_2$ is also band-limited.

In Appendix B, we provide the extension of the $M(2)$-Fourier transform to the space of all rapidly decreasing functions $\mathcal{S}(M(2))$ and tempered distributions $\mathcal{S}'(M(2))$ defined on $M(2)$.

3. Exponential radon transform inversion using $M(2)$-Fourier transform

3.1. Exponential Radon Transform as a Convolution over $M(2)$. Let $\mu \in \mathbb{C}$. The exponential Radon transform of a compactly supported real valued function f over $\mathbb{R}^2$ is given by

$$\mathcal{T}_\mu f(\boldsymbol{\vartheta}, -r_1) = \int_{\mathbb{R}^2} f(\boldsymbol{x})\delta(\boldsymbol{x}\cdot\boldsymbol{\vartheta} + r_1)\mathrm{e}^{\mu \boldsymbol{x}\cdot\boldsymbol{\vartheta}^\perp} d\boldsymbol{x}. \tag{23}$$

Multiplying the exponential Radon transform of f with $\mathrm{e}^{\mu r_2}$, $r_2 \in \mathbb{R}$, the resulting integral can be expressed as a convolution operation over $M(2)$:

$$\begin{aligned}
\mathcal{T}'_\mu f(g) = \mathrm{e}^{\mu r_2}\mathcal{T}_\mu f(\boldsymbol{\vartheta}, -r_1) &= \int_{\mathbb{R}^2} f(\boldsymbol{x})\delta(\boldsymbol{x}\cdot\boldsymbol{\vartheta} + r_1)\mathrm{e}^{\mu\, \boldsymbol{x}\cdot\boldsymbol{\vartheta}^\perp + \mu r_2} d\boldsymbol{x} \\
&= \int_{\mathbb{R}^2} f(\boldsymbol{x})\delta(R_\theta \boldsymbol{x}\cdot\boldsymbol{e_1} + r_1)\mathrm{e}^{\mu\, R_\theta \boldsymbol{x}\cdot\boldsymbol{e_2} + \mu r_2} d\boldsymbol{x} \\
&= \int_{\mathbb{R}^2} f(\boldsymbol{x})\delta((R_\theta \boldsymbol{x} + \boldsymbol{r})\cdot\boldsymbol{e_1})\mathrm{e}^{\mu\,(R_\theta \boldsymbol{x} + \boldsymbol{r})\cdot\boldsymbol{e_2}} d\boldsymbol{x} \\
&= \frac{1}{2\pi}\int_0^{2\pi}\int_{\mathbb{R}^2} f(\boldsymbol{x})\delta((R_\theta \boldsymbol{x} + \boldsymbol{r})\cdot\boldsymbol{e_1})\mathrm{e}^{\mu\,(R_\theta \boldsymbol{x} + \boldsymbol{r})\cdot\boldsymbol{e_2}} d\boldsymbol{x} d\phi \\
&= \int_{M(2)} f(h)\Lambda(gh) d(h) \\
&= (\Lambda *_{M(2)} f^*)(g), \quad g = (R_\theta, \boldsymbol{r}) \in M(2),
\end{aligned} \tag{24}$$

where $f^*(g) = \overline{f(g^{-1})}$. Λ will be called the convolution filter which is given by

$$\Lambda(h) = \delta(\boldsymbol{x}\cdot\boldsymbol{e_1})\mathrm{e}^{\mu\, \boldsymbol{x}\cdot\boldsymbol{e_2}}, \quad h = (R_\phi, \boldsymbol{x}) \in M(2). \tag{25}$$

Note that the exponential Radon transform $\mathcal{T}_\mu f$ can be viewed as a restriction of the convolution $\Lambda *_{M(2)} f^*$

$$\begin{aligned}
(\Lambda *_{M(2)} f^*)(g)\big|_{r_2=0} &= \mathcal{T}_\mu f(\boldsymbol{\vartheta}, -r_1)\mathrm{e}^{\mu\, r_2}\big|_{r_2=0} \\
&= \mathcal{T}_\mu f(\boldsymbol{\vartheta}, -r_1), \quad g = (R_\theta, \boldsymbol{r}),
\end{aligned} \tag{26}$$

where $\boldsymbol{r} = (r_1, r_2)^T$ and $\boldsymbol{\vartheta} = {R_\theta}^T \boldsymbol{e_1}$.

We extended the convolution representation to the angle dependent exponential Radon transform in Appendix C.1. The corresponding convolution formula is given by

$$\mathcal{T}'_\mu f(g) = (\Lambda *_{M(2)} f^*_\delta)(g), \quad g = (R_\theta, \boldsymbol{r}) \in M(2), \tag{27}$$

where $f_\delta(h) = f(\boldsymbol{x})\delta(\phi)$, and $\Lambda(h) = \delta(\boldsymbol{x}\cdot\boldsymbol{e_1})\mathrm{e}^{\mu(-\phi)\,\boldsymbol{x}\cdot\boldsymbol{e_2}}$, $h = (R_\phi, \boldsymbol{x}) \in M(2)$.

In Appendix C.2 we show that the half-scan problem can be expressed as a deconvolution over $M(2)$ by using the angle-dependent exponential Radon transform.

The inversion approach introduced in the following sections can potentially address the inversion of the angle-dependent exponential Radon transform. However, this is beyond the scope of the current paper. For the rest of our discussion, we will focus on the inversion of the exponential Radon transform with uniform attenuation.

3.2. Exponential Radon Transform Inversion. Treating the projections $\mathcal{T}'_\mu f$ and the filter Λ as tempered distributions, the modified exponential Radon transform can be expressed as a multiplication in the $M(2)$-Fourier transform domain (Appendix B). Using the convolution property of the $M(2)$-Fourier transform, (24) becomes

$$\widehat{\mathcal{T}'_\mu f}(\lambda) = \hat{f}^\dagger(\lambda)\hat{\Lambda}(\lambda), \quad \lambda \geq 0 \tag{28}$$

or in matrix elements

$$\widehat{\mathcal{T}'_\mu f}_{mn}(\lambda) = \sum_q \overline{\hat{f}_{qm}(\lambda)}\hat{\Lambda}_{qn}(\lambda), \quad m, n \in \mathbb{Z}. \tag{29}$$

Equation (29) provides a block diagonal representation of the modified exponential Radon transform in the $M(2)$-Fourier domain, where each block is indexed by $\lambda \geq 0$. We will show that various treatments of (29) leads to different reconstruction algorithms.

Treating (29) as an operator multiplication, the $M(2)$-Fourier coefficients of f can be expressed as

$$\hat{f}(\lambda) = \left[\hat{\Lambda}^\dagger(\lambda)\right]^{-1} \widehat{\mathcal{T}'_\mu f}^\dagger(\lambda). \tag{30}$$

Note that $\hat{\Lambda}$ is a rank one operator, hence, it is compact. Therefore, its inverse exists, but not bounded [14]. In order to obtain a stable but approximate inverse $\widehat{\Lambda_\mu}$ has to be regularized [15]. Thus, we replace $\left[\hat{\Lambda}^\dagger(\lambda)\right]^{-1}$ with its regularized linear least square approximation:

$$\hat{f}(\lambda) = \hat{\Lambda}(\lambda)\left[\hat{\Lambda}^\dagger(\lambda)\hat{\Lambda}(\lambda) + \sigma I\right]^{-1} \widehat{\mathcal{T}'_\mu f}^\dagger(\lambda), \tag{31}$$

where σ is a small positive number and I is the identity operator. The regularized inverse given in (31) is a special case of the Wiener filter developed in [10]. The regularization parameter σ can be interpreted as the ratio of the noise variance to the image variance. Note that $\left[\hat{\Lambda}^\dagger(\lambda)\hat{\Lambda}(\lambda) + \sigma I\right]^{-1}$ in (31) is the zeroth order Tikhonov regularized inverse of $\hat{\Lambda}^\dagger(\lambda)\hat{\Lambda}(\lambda)$, and $\hat{\Lambda}(\lambda)\left[\hat{\Lambda}^\dagger(\lambda)\hat{\Lambda}(\lambda) + \sigma I\right]^{-1}$ converges to the Moore-Penrose generalized inverse of $\hat{\Lambda}^\dagger(\lambda)$ as $\sigma \to 0$ [15, 16].

Formula (31) gives rise to Algorithm 3, described in Section 5.

Alternatively, since $\hat{\Lambda}$ is $SO(2)$ invariant, all the rows of the matrix representation $\hat{\Lambda}_{mn}$, except 0^{th} row, is equal to zero. Thus the only contribution to the summation (29) is from $q = 0$. As long as $\hat{\Lambda}_{0n}(\lambda) \neq 0$, (29) can be simplified to

$$\widehat{\mathcal{T}'_\mu f}_{mn}(\lambda) = \overline{\hat{f}_{0m}(\lambda)}\hat{\Lambda}_{0n}(\lambda), \tag{32}$$

providing an alternative formula for the computation of $M(2)$-Fourier coefficients of f:

$$\hat{f}_{0m}(\lambda) = \overline{\left(\frac{\widehat{\mathcal{T}'_\mu f}_{mn}(\lambda)}{\hat{\Lambda}_{0n}(\lambda)} \right)}, \quad m \in \mathbb{Z}. \tag{33}$$

Note that the left hand side of (33), $\hat{f}_{0m}(\lambda)$, is independent of n, while the right hand side of (33) depends on n. This means that for each $n \in \mathbb{Z}$, (33) provides a method to compute the $M(2)$-Fourier transform of f from the $M(2)$-Fourier transforms of its modified projections $\mathcal{T}'_\mu f$. For a fixed $n = n_0$, formula (33) gives rise to Algorithm 1, described in Section 5. Further analysis of formula (33) in Section 4 shows that it leads to a new class of relationships between the circular harmonic decomposition of the Fourier transform of the function f and its projections.

Alternatively, (33) can be treated as an over determined linear system of equations, for a given set of n values $\{n_1, n_2, \ldots\} \subset \mathbb{Z}$:

$$\begin{bmatrix} \widehat{\mathcal{T}_\mu f}_{mn_1}(\lambda) \\ \widehat{\mathcal{T}_\mu f}_{mn_2}(\lambda) \\ \vdots \end{bmatrix} = \overline{\hat{f}_{0m}(\lambda)} \begin{bmatrix} \hat{\Lambda}_{0n_1}(\lambda) \\ \hat{\Lambda}_{0n_2}(\lambda) \\ \vdots \end{bmatrix}. \tag{34}$$

Then, the computation of the linear least square solution of $\hat{f}_{0m}(\lambda)$ gives rise to Algorithm 2 of Section 5:

$$\hat{f}_{0m}(\lambda) = \frac{\sum_{n \in \{n_0, n_1, \ldots\}} \overline{\widehat{\mathcal{T}'_\mu f}_{mn}(\lambda)} \hat{\Lambda}_{0n}(\lambda)}{\sum_{n \in \{n_0, n_1, \ldots\}} \overline{\hat{\Lambda}_{0n}(\lambda)} \hat{\Lambda}_{0n}(\lambda)}. \tag{35}$$

The reconstruction formulae (31), (33) and (35) are summarized in Table 1.

Formula	**Equation #**	**Method #**
$\hat{f}_{0m}(\lambda) = \overline{\left(\frac{\widehat{\mathcal{T}'_\mu f}_{mn}(\lambda)}{\hat{\Lambda}_{0n_0}(\lambda)} \right)}$	(33)	1
$\hat{f}_{0m}(\lambda) = \frac{\sum_{n \in \{n_0, n_1, \ldots\}} \overline{\widehat{\mathcal{T}'_\mu f}_{mn}(\lambda)} \hat{\Lambda}_{0n}(\lambda)}{\sum_{n \in \{n_0, n_1, \ldots\}} \overline{\hat{\Lambda}_{0n}(\lambda)} \hat{\Lambda}_{0n}(\lambda)}$	(35)	2
$\hat{f}(\lambda) = \hat{\Lambda}(\lambda) \left[\hat{\Lambda}^\dagger(\lambda) \hat{\Lambda}(\lambda) + \sigma I \right]^{-1} \widehat{\mathcal{T}'_\mu f}^\dagger(\lambda)$	(31)	3

TABLE 1. Computing the $M(2)$-Fourier coefficients of f

After $\hat{f}$ is computed by either of the formulae (31), (33) or (35) , f can be reconstructed using the inverse $M(2)$-Fourier transform:

$$f(\boldsymbol{x}) = \mathcal{F}^{-1}_{M(2)} \left(\hat{f}(\lambda) \right) = \int_0^\infty \sum_m \hat{f}_{0m}(\lambda) u^{(\lambda)}_{m0}(h) \lambda d\lambda. \tag{36}$$

4. Analysis of formula (33)

In this section, we will show that analysis of (33) leads to a class of relationships between the circular harmonic decompositions of the Fourier transform of the function and its projections. These relationships are obtained by substituting the $M(2)$-Fourier transform of the convolution filter Λ and the modified projections $\mathcal{T}'_\mu f$ into (33).

4.1. Computation of the $M(2)$-Fourier coefficients of $\Lambda(g)$. Let $\Lambda(g) = \delta(\boldsymbol{r}\cdot\boldsymbol{e_1})\mathrm{e}^{\mu\,\boldsymbol{r}\cdot\boldsymbol{e_2}}$. Then $M(2)$-Fourier transform of Λ is given by

$$\begin{aligned}\hat{\Lambda}_{mn}(\lambda) &= \int_{M(2)} \delta(r_1)\mathrm{e}^{\mu\, r_2} \int_{S^1} S_n(\boldsymbol{s})\mathrm{e}^{\mathrm{i}\lambda\boldsymbol{r}\cdot\boldsymbol{s}}\overline{S_m(R_\theta^{-1}\boldsymbol{s})}d(\boldsymbol{s})d(g)\\ &= \delta_{0m}\int_{S^1}\int_{\mathbb{R}} \mathrm{e}^{\mu\, r_2}\mathrm{e}^{\mathrm{i}\lambda r_2 s_2} dr_2 S_n(\boldsymbol{s})d(\boldsymbol{s})\\ &= \delta_{0m}\int_0^{2\pi} \delta(\lambda\sin\varphi - \mathrm{i}\mu)\mathrm{e}^{\mathrm{i}n\varphi}d\varphi \qquad (37)\end{aligned}$$

where $\delta(.)$ is the delta function over $\mathbb{C}$ (see page 160, Equation (6) and page 169 Equation (8) of [17]) defined as $\langle\delta(s+h),\phi(s)\rangle = \phi(h)$, for all $s,h\in\mathbb{C}$. Since $\delta(f(x)) = \sum_n \frac{1}{|f'(x_n)|}\delta(x-x_n)$, x_n being the roots of f (see page 184, Equations (I–IV) of [17]). Hence, for any $\mu\in\mathbb{C}$, $\hat{\Lambda}_{mn}(\lambda)$ can be computed as follows:

$$\hat{\Lambda}_{mn}(\lambda) = \delta_{0m}\frac{1}{\lambda}\sum_{\varphi_0}\mathrm{e}^{\mathrm{i}n\varphi_0} \qquad (38)$$

where φ_0 is in the support of $\delta\left(-\mathrm{i}\mu/\lambda + \sin\varphi\right)$ given by

$$\varphi_0 = \arcsin(\mathrm{i}\mu/\lambda) = -\mathrm{i}\ln(-\mu/\lambda \pm \sqrt{1+\mu^2/\lambda^2}). \qquad (39)$$

Thus,

$$\cos\varphi_0 = \pm\sqrt{1+\mu^2/\lambda^2}. \qquad (40)$$

Substituting (39) and (40) in (38), we obtain

$$\hat{\Lambda}_{mn}(\lambda) = \delta_{0m}\lambda^{-(n+1)}\left((-1)^n(\sqrt{\mu^2+\lambda^2}+\mu)^n + (\sqrt{\mu^2+\lambda^2}-\mu)^n\right). \qquad (41)$$

4.2. Computation of the $M(2)$-Fourier coefficients of $\mathcal{T}'_\mu f(g)$. We will use the notations $\mathcal{T}_\mu f(\boldsymbol{\theta}, r)$ and $\mathcal{T}_\mu f(\theta, r)$ interchangeably.

Let $\widetilde{\mathcal{T}_\mu f}(\theta,\sigma)$ denote the 1-dimensional standard Fourier transform of $\mathcal{T}_\mu f(\theta, r)$, i.e.

$$\widetilde{\mathcal{T}_\mu f}(\theta,\sigma) = \int_{\mathbb{R}} \mathcal{T}_\mu f(\theta, r)\mathrm{e}^{-\mathrm{i}\sigma r}\, dr. \qquad (42)$$

Let $\widetilde{\mathcal{T}_\mu f}$ denote the circular harmonic decomposition of $\widetilde{\mathcal{T}_\mu f}(\theta,\sigma)$, i.e.

$$\widetilde{\mathcal{T}_\mu f}_m(\sigma) = \int_{S^1} \widetilde{\mathcal{T}_\mu f}(\boldsymbol{\omega},\sigma)S_m(\boldsymbol{\omega})\, d(\boldsymbol{\omega}). \qquad (43)$$

Since $\mathcal{T}_\mu f(\boldsymbol{\vartheta}, r) = \mathcal{T}_\mu f(-\theta, r)$, the $M(2)$-Fourier coefficients of $\mathcal{T}'_\mu f(g)$ are

$$\begin{aligned}\widehat{\mathcal{T}'_\mu f}_{mn}(\lambda) &= \int_{M(2)} \mathrm{e}^{\mu r_2} \mathcal{T}_\mu f(\boldsymbol{\vartheta}, -r_1) \int_{S^1} S_n(\boldsymbol{s}) \mathrm{e}^{\mathrm{i}\lambda \boldsymbol{r}\cdot\boldsymbol{s}} \overline{S_m(R_\theta^{-1}\boldsymbol{s})} d(\boldsymbol{s}) d(g) \\ &= \frac{1}{2\pi}\int_0^{2\pi} \int_{\mathbb{R}} \mathrm{e}^{(\mu + \mathrm{i}\lambda\sin\varphi) r_2} dr_2 \frac{1}{2\pi}\int_0^{2\pi} \widetilde{\mathcal{T}_\mu f}(-\theta, \lambda\cos\varphi) \mathrm{e}^{\mathrm{i}m\theta} d\theta \mathrm{e}^{\mathrm{i}(n-m)\varphi} d\varphi \\ &= \int_0^{2\pi} \delta(-\mathrm{i}\mu + \lambda\sin\varphi) \widetilde{\mathcal{T}_\mu f}_{-m}(\lambda\cos\varphi) \mathrm{e}^{\mathrm{i}(n-m)\varphi} d\varphi. \qquad (44)\end{aligned}$$

Then (44) can be written as follows:

$$\widehat{\mathcal{T}'_\mu f}_{mn}(\lambda) = \frac{1}{\lambda} \sum_{\varphi_0} \widetilde{\mathcal{T}_\mu f}_{-m}(\lambda\cos\varphi_0) \mathrm{e}^{\mathrm{i}(n-m)\varphi_0}, \qquad (45)$$

where φ_0 is in the support of $\delta(-\mathrm{i}\mu/\lambda + \sin\varphi)$. Substituting (39) and (40) in (45), we obtain

$$\begin{aligned}\widehat{\mathcal{T}'_\mu f}_{mn}(\lambda) =& \frac{1}{\lambda^{n-m+1}} \left[\widetilde{\mathcal{T}_\mu f}_{-m}(\sqrt{\lambda^2+\mu^2}) \left(-\mu + \sqrt{\lambda^2+\mu^2}\right)^{n-m} \right. \\ &\left. + \widetilde{\mathcal{T}_\mu f}_{-m}(-\sqrt{\lambda^2+\mu^2}) \left(-\mu - \sqrt{\lambda^2+\mu^2}\right)^{n-m} \right]. \qquad (46)\end{aligned}$$

4.3. A Class of Relationships Based on Formula (33). Substituting the $M(2)$-Fourier coefficients of Λ and $\mathcal{T}'_\mu f$ ((38) and (46), respectively) into (33), and using the $SO(2)$ invariance property of the $M(2)$-Fourier transform, the circular harmonic decomposition of the Fourier transform of f can be expressed as

$$\begin{aligned}\widetilde{f}_{-m}(\lambda) =& \widetilde{\mathcal{T}_\mu f}_{-m}(\sqrt{\lambda^2+\mu^2}) \frac{\lambda^m \left(-\mu + \sqrt{\lambda^2+\mu^2}\right)^{n-m}}{(-1)^n(\sqrt{\mu^2+\lambda^2}+\mu)^n + (\sqrt{\mu^2+\lambda^2}-\mu)^n} \\ &+ \widetilde{\mathcal{T}_\mu f}_{-m}(-\sqrt{\lambda^2+\mu^2}) \frac{\lambda^m \left(-\mu - \sqrt{\lambda^2+\mu^2}\right)^{n-m}}{(-1)^n(\sqrt{\mu^2+\lambda^2}+\mu)^n + (\sqrt{\mu^2+\lambda^2}-\mu)^n}, \qquad (47)\end{aligned}$$

for any integer n. Note that since for any real valued function f, $\widetilde{f}_m(-\lambda) = \overline{\widetilde{f}_{-m}(\lambda)}$ for $\lambda \geq 0$, (47) is valid for any $\lambda \in \mathbb{R}$.

In [5], it was argued that the circular harmonic decomposition of the Fourier transform of f can be expressed as a linear combination of $\widetilde{\mathcal{T}'_\mu f}_{-m}(\sqrt{\lambda^2+\mu^2})$ and $\widetilde{\mathcal{T}'_\mu f}_{-m}(-\sqrt{\lambda^2+\mu^2})$ and the following formula is proposed (formula (35) in [5]):

$$\widetilde{f}_k(\lambda) = \omega\gamma_\mu(\lambda)^k \widetilde{\mathcal{T}_\mu f}_k(\sqrt{\mu^2+\lambda^2}) + (1-\omega)(-1)^k \gamma_\mu(\lambda)^{-k} \widetilde{\mathcal{T}_\mu f}_k(-\sqrt{\mu^2+\lambda^2}), \qquad (48)$$

where $\gamma_\mu(\lambda) = \frac{\lambda}{\sqrt{\mu^2+\lambda^2}+\mu}$ and ω is a weighting function. It was shown that various choices of ω lead to inversion methods described in [7, 3, 8]. It was also argued that the frequency dependent weighting function ω may lead to optimal reconstruction.

Setting $\rho_n = \frac{\gamma_\mu(\lambda)^n}{(-1)^n\gamma_\mu(\lambda)^{-n} + \gamma_\mu(\lambda)^n}$ and $k = -m$, (47) can be put in a form similar to (48):

$$\widetilde{f}_k(\lambda) = \rho_n\gamma_\mu(\lambda)^k \widetilde{\mathcal{T}_\mu f}_k(\sqrt{\mu^2+\lambda^2}) + (1-\rho_n)(-1)^k \gamma_\mu(\lambda)^{-k} \widetilde{\mathcal{T}_\mu f}_k(-\sqrt{\mu^2+\lambda^2}). \qquad (49)$$

Remarks.

1. The weighted summation formula (49) is due to the $M(2)$-invariance of the exponential Radon transform.
2. For each $n \in \mathbb{Z}$, (49) provides a relationship between $\widetilde{f}_{-m}$ and $\widetilde{\mathcal{T}_\mu f}_{-m}$, $m \in \mathbb{Z}$. Here, n is the column index and m is the row index of the matrix representation of the $M(2)$-Fourier transform of $\mathcal{T}'_\mu f$. Therefore the indices $k = -m$ and n in (49) are independent unlike formula (42) in [5].
3. When there is no noise, the optimal weights proposed in formula (40) of [5] can be obtained by choosing $n = 2k$ in (49).
4. While Algorithm 1 is based on a single index n_0 in formula (49), Algorithm 2, and 3 inherently combine all $n \in \mathbb{Z}$ relationships in (49). Numerical simulations show that the later approaches provide better performance.
5. $M(2)$-Fourier transform allows *simultaneous* computation of all the relationships $(n, k \in \mathbb{Z})$ in (49).

In the next section, we will present the reconstruction algorithms based on the formulas (31), (33) and (35).

5. Reconstruction algorithms and numerical simulations

5.1. Reconstruction Algorithms. The proposed exponential Radon transform inversion algorithms are based on either the formula (31), (33) or (35), and can be implemented in four steps as shown in the following diagram:

(50)
$$\begin{array}{ccccc} f & \xrightarrow{\mathcal{T}} & \mathcal{T}_\mu f & \xrightarrow[1]{\times\, e^{\mu r_2}} & \mathcal{T}'_\mu f \\ & \nwarrow^{4} & & & \downarrow{\scriptstyle 2}\ \mathcal{F}_{M(2)} \\ & \mathcal{F}^{-1}_{M(2)} \searrow & & & \\ & & \hat{f}_{0m} & \xleftarrow[3]{\hat{\Lambda}^{-1}_{0n}} & \widehat{\mathcal{T}'_\mu f}_{mn} \end{array} .$$

The first step involves modification of the projections that extend the projections from $\mathbb{R} \times S^1$ to $M(2)$. The second step involves computation of the $M(2)$-Fourier transform of the modified projections. The third step involves computation of the $M(2)$-Fourier transform of f from its modified projections given the filter Λ. Finally, the fourth step involves computation of the function f using the inverse $M(2)$-Fourier transform.

Let $f(\boldsymbol{x}) = 0$ for $|\boldsymbol{x}| > a$ and hence $\mathcal{T}_\mu f(\theta, r_1) = 0$ for $|r_1| > a$. The four step reconstruction algorithms can be implemented as follows:

Step 1. Extend $\mathcal{T}_\mu f(\theta, -r_1)$ to $\mathcal{T}'_\mu f(g)$ by multiplying with $e^{\mu r_2}$ for $r_2 \in [-a, a]$, where $0 < a < \infty$.

Step 2. Compute $\widehat{\mathcal{T}'_\mu f}_{mn}(\lambda)$, the $M(2)$-Fourier transform of $\mathcal{T}'_\mu f$ for $m, n = 0, \pm 1, \ldots, \pm K$, and $\lambda = \frac{k\lambda_0}{K+1}$, $k = 0, \ldots, K$ for some $\lambda_0 > 0$.

Step 3. Compute $\hat{f}_{0m}(\lambda)$ by either of the following ways:

Algorithm 1. For fixed $n = n_0$, and for each λ, compute $\hat{f}_{0m}(\lambda)$ for each m by

(51)
$$\hat{f}_{0m}(\lambda) = \overline{\left(\frac{\widehat{\mathcal{T}'_\mu f}_{mn_0}(\lambda)}{\hat{\Lambda}_{0n_0}(\lambda) + \sigma} \right)},$$

where σ is a small positive constant.

Algorithm 2. For a given subset $\{n_1, n_2, \ldots\}$ of $\{-K, \ldots, K\}$, and for each λ, let $[\hat{\Lambda}_0(\lambda)]$ and $[\widehat{\mathcal{T}'_\mu f}_m(\lambda)]$ denote the row vectors given by

$$[\hat{\Lambda}_0(\lambda)] = \begin{bmatrix} \hat{\Lambda}_{0n_1}(\lambda) & \hat{\Lambda}_{0n_2}(\lambda) & \ldots \end{bmatrix} \tag{52}$$

$$[\widehat{\mathcal{T}'_\mu f}_m(\lambda)] = \begin{bmatrix} \widehat{\mathcal{T}'_\mu f}_{mn_1}(\lambda) & \widehat{\mathcal{T}'_\mu f}_{mn_2}(\lambda) & \ldots \end{bmatrix}. \tag{53}$$

Then for each m, compute $\hat{f}_{0m}(\lambda)$ by

$$\hat{f}_{0m}(\lambda) = \frac{\overline{[\widehat{\mathcal{T}'_\mu f}_m(\lambda)]}[\hat{\Lambda}_0(\lambda)]^T}{\overline{[\hat{\Lambda}_0(\lambda)]}[\hat{\Lambda}_0(\lambda)]^T + \sigma}, \tag{54}$$

where the superscript ^{T} denotes the transpose operation and σ is a small positive constant.

Algorithm 3. For each λ, let $[\hat{\Lambda}(\lambda)]$, $[\widehat{\mathcal{T}'_\mu f}(\lambda)]$ and $[\hat{f}(\lambda)]$ denote the $2K+1$ by $2K+1$ matrices given by

$$[\hat{\Lambda}(\lambda)] = \begin{bmatrix} 0 & \cdots & 0 & 0 & 0 & \cdots & 0 \\ \vdots & & \vdots & \vdots & \vdots & & \vdots \\ 0 & \cdots & 0 & 0 & 0 & \cdots & 0 \\ \hat{\Lambda}_{0(-K)} & \cdots & \hat{\Lambda}_{0(n-1)}(\lambda) & \hat{\Lambda}_{0n}(\lambda) & \hat{\Lambda}_{0n+1}(\lambda) & \cdots & \hat{\Lambda}_{0K} \\ 0 & \cdots & 0 & 0 & 0 & \cdots & 0 \\ \vdots & & \vdots & \vdots & \vdots & & \vdots \\ 0 & \cdots & 0 & 0 & 0 & \cdots & 0 \end{bmatrix} \tag{55}$$

$$[\widehat{\mathcal{T}'_\mu f}(\lambda)] = \begin{bmatrix} \widehat{\mathcal{T}'_\mu f}_{(-K)(-K)}(\lambda) & \widehat{\mathcal{T}'_\mu f}_{(-K)(-K+1)}(\lambda) & \cdots & \widehat{\mathcal{T}'_\mu f}_{(-K)K}(\lambda) \\ \widehat{\mathcal{T}'_\mu f}_{(-K+1)(-K)}(\lambda) & \widehat{\mathcal{T}'_\mu f}_{(-K+1)(-K+1)}(\lambda) & \cdots & \widehat{\mathcal{T}'_\mu f}_{(-K+1)K}(\lambda) \\ \vdots & \vdots & \ddots & \vdots \\ \widehat{\mathcal{T}'_\mu f}_{K(-K)}(\lambda) & \widehat{\mathcal{T}'_\mu f}_{K(-K+1)}(\lambda) & \cdots & \widehat{\mathcal{T}'_\mu f}_{KK}(\lambda) \end{bmatrix} \tag{56}$$

$$[\hat{f}(\lambda)] = \begin{bmatrix} 0 & \cdots & 0 & 0 & 0 & \cdots & 0 \\ \vdots & & \vdots & \vdots & \vdots & & \vdots \\ 0 & \cdots & 0 & 0 & 0 & \cdots & 0 \\ \hat{f}_{0(-K)} & \cdots & \hat{f}_{0(n-1)}(\lambda) & \hat{f}_{0n}(\lambda) & \hat{f}_{0n+1}(\lambda) & \cdots & \hat{f}_{0K} \\ 0 & \cdots & 0 & 0 & 0 & \cdots & 0 \\ \vdots & & \vdots & \vdots & \vdots & & \vdots \\ 0 & \cdots & 0 & 0 & 0 & \cdots & 0 \end{bmatrix} \tag{57}$$

Then

$$[\hat{f}(\lambda)] \approx [\hat{\Lambda}(\lambda)] \left(\overline{[\hat{\Lambda}(\lambda)]}^T [\hat{\Lambda}(\lambda)] + \sigma I \right)^{-1} \overline{[\widehat{\mathcal{T}'_\mu f}(\lambda)]}^T, \tag{58}$$

where σ is a positive constant close to zero. Note that a generalization of *Algorithm 3* for $\mu = 0$ was presented in our earlier work [18].

Step 4. Take the inverse $M(2)$-Fourier transform of $\hat{f}_{mn}(\lambda)$ to obtain f.

For numerical simulations, a fast implementation of the $M(2)$-Fourier transform based on (15) was implemented as described in [9, 18, 19, 20]. If there are K number of samples in each of S^1 and $\mathbb{R}$, the computational complexity of the $M(2)$-Fourier transform is $\mathcal{O}(K^3 \log K)$. Although the θ independence of the function f reduces the computational complexity of the inverse $M(2)$-Fourier transform of $\hat{f}_{mn}(\lambda)$ to $\mathcal{O}(K^2 \log K)$, the overall computational complexity of the algorithms is dominated by the computation of the $M(2)$-Fourier coefficients of the extended projections $\mathcal{T}'_\mu f$, which has a computational complexity of $\mathcal{O}(K^3 \log K)$.

5.2. Performance of the Reconstruction Algorithms. We study the behavior of the weighting factors in (49) to understand the performance of the reconstruction algorithms. Let us rewrite (49) as

$$\widetilde{f}_k(\lambda) = \eta_{(n,k)}(\lambda)\widetilde{\mathcal{T}_\mu f}_k(\sqrt{\lambda^2+\mu^2}) + \eta_{(-n,-k)}(\lambda)(-1)^k\widetilde{\mathcal{T}_\mu f}_k(-\sqrt{\lambda^2+\mu^2}) \tag{59}$$

where $\eta_{(n,k)}(\lambda)$ is the weight of $\widetilde{\mathcal{T}_\mu f}_k(\sqrt{\lambda^2+\mu^2})$ given by

$$\eta_{(n,k)}(\lambda) = \rho_n\gamma^k = \frac{\left(\sqrt{\lambda^2+\mu^2}-\mu\right)^{n+k}}{\lambda^k\left[(-1)^n(\sqrt{\lambda^2+\mu^2}+\mu)^n + (\sqrt{\lambda^2+\mu^2}-\mu)^n\right]}. \tag{60}$$

We investigate the behavior of $\eta_{(n,k)}(\lambda)$ and $\eta_{(-n,-k)}(\lambda)$ and their derivative with respect to λ for various values of n and k as λ goes to 0 and ∞, first, for $0 < \mu \in \mathbb{R}$ and next for $\mu = \mathrm{i}\beta$, $0 < \beta \in \mathbb{R}$.

It can be easily verified that when $\mu > 0$,

$$\begin{array}{lll} \eta_{(n,k)}(\lambda) > 0, & & n \in 2\mathbb{Z} \\ \eta_{(n,k)}(\lambda) < 0, & n > 0, & n \in 2\mathbb{Z}+1 \\ \eta_{(n,k)}(\lambda) > 0, & n < 0, & n \in 2\mathbb{Z}+1 \end{array}. \tag{61}$$

The limit of $\eta_{(n,k)}(\lambda)$ as λ goes to infinity is

$$\lim_{\lambda\longrightarrow\infty}\eta_{(n,k)}(\lambda) = \begin{cases} \frac{1}{2} & n \in 2\mathbb{Z} \\ -\operatorname{sgn}(n)\infty & n \in 2\mathbb{Z}+1 \end{cases}. \tag{62}$$

Furthermore, for $k > 0$, it is straight forward to show that,

$$\lim_{\lambda\longrightarrow 0}\eta_{(n,k)}(\lambda) = 0, \tag{63}$$

and the derivative of $\eta_{(n,k)}(\lambda)$ with respect to λ satisfies

$$\begin{array}{ll} \frac{\mathrm{d}\eta_{(n,k)}(\lambda)}{\mathrm{d}\lambda} < 0, & n > 0 \\ \frac{\mathrm{d}\eta_{(n,k)}(\lambda)}{\mathrm{d}\lambda} > 0, & n < 0 \end{array}, \quad n \in 2\mathbb{Z}+1 \qquad \frac{\mathrm{d}\eta_{(n,k)}(\lambda)}{\mathrm{d}\lambda} > 0, \quad n \in 2\mathbb{Z}. \tag{64}$$

Hence, for $k > 0$, $\eta_{(n,k)}(\lambda)$ (for $k < 0$, $\eta_{(n,-k)}(\lambda)$) behaves like a high-pass filter for $\widetilde{\mathcal{T}_\mu f}_k(\sqrt{\lambda^2+\mu^2})$ $\left(\widetilde{\mathcal{T}_\mu f}_k(-\sqrt{\lambda^2+\mu^2})\right)$, for all n. However, for $n \in 2\mathbb{Z}+1$, it behaves more like a ramp filter, the higher the frequency the more it amplifies. For $n \in 2\mathbb{Z}$, on the other hand, $\eta_{(n,k)}(\lambda)$ converges to $\frac{1}{2}$, amplifying the high frequency content of $\widetilde{\mathcal{T}_\mu f}_k$ almost uniformly. As a result, high frequency error in numerical computation or noise is amplified by $\eta_{(n,k)}(\lambda)$ when n is odd but tapered off when n is even valued. Figure 1 illustrates the behavior of $|\eta_{(n,k)}(\lambda)|$.

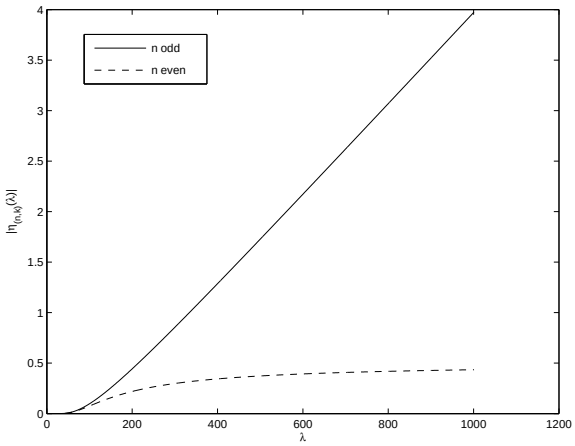

FIGURE 1. Illustrative plot for $|\eta_{(n,k)}(\lambda)|$, $k > 0$. Solid and dashed lines correspond to $|\eta_{(n,k)}(\lambda)|$ for odd and even n values, respectively.

Secondly, for imaginary $\mu = \mathrm{i}\beta$, $0 < \beta \in \mathbb{R}$,

$$\eta_{(n,k)}(\lambda) = \begin{cases} \dfrac{\sqrt{1-\frac{\beta^2}{\lambda^2}}\ \exp\left(-\mathrm{i}(n+k)\arctan\left(\frac{\beta}{\sqrt{\lambda^2-\beta^2}}\right)\right)}{2\cos\left(n\arctan\left(\frac{\beta}{\sqrt{\lambda^2-\beta^2}}\right)\right)}, & n \in 2\mathbb{Z} \\ \dfrac{\sqrt{1-\frac{\beta^2}{\lambda^2}}\ \exp\left(-\mathrm{i}(n+k)\arctan\left(\frac{\beta}{\sqrt{\lambda^2-\beta^2}}\right)\right)}{2\mathrm{i}\sin\left(n\arctan\left(\frac{\beta}{\sqrt{\lambda^2-\beta^2}}\right)\right)}, & n \in 2\mathbb{Z}+1 \end{cases} . \tag{65}$$

Thus, for imaginary μ, $\eta_{(n,k)}(\lambda)$ is complex valued and oscillatory. The oscillatory behavior of $\eta_{(n,k)}(\lambda)$ increases as absolute value of n increases. Due to this oscillatory behavior, $\eta_{(n,k)}(\lambda)$ amplifies the high frequencies in an oscillatory manner.

The two cases discussed above can be extended for any real or imaginary attenuation. While for both real and imaginary μ, the behavior of $\eta_{(n,k)}(\lambda)$ for high frequencies is

$$\lim_{\lambda\longrightarrow\infty} \left|\eta_{(n,k)}(\lambda)\right| = \lim_{\lambda\longrightarrow\infty} \left|\eta_{(-n,-k)}(\lambda)\right| = \begin{cases} \frac{1}{2} & n \in 2\mathbb{Z} \\ \infty & n \in 2\mathbb{Z}+1. \end{cases}, \qquad n > 0, \tag{66}$$

the behavior of convergence is different. This difference is observed in the reconstructed images [20, 21, 22].

5.3. Numerical Simulations.

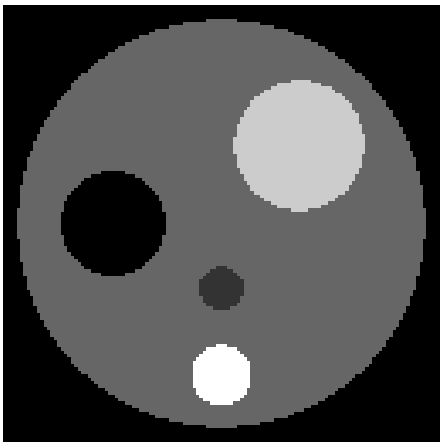

FIGURE 2. The numerical phantom defined by the parameters in Table 2

FIGURE 3. Reconstruction of the phantom using Algorithm 1 with $n = 0$, with $\mu = 0.154\text{cm}^{-1}$ and $\sigma = 10^{-8}$.

5.3.1. *Analytic computation of the projections.* Making the change of variable $\boldsymbol{x} = s\boldsymbol{\theta} + t\boldsymbol{\theta}^{\perp}$, the exponential Radon transform of a disk f with unit emission distribution and radius r_0 can be computed by

$$\begin{aligned} \mathcal{T}_\mu f(\boldsymbol{\theta}, s) &= \int_{\mathbb{R}} f(s\boldsymbol{\theta} + t\boldsymbol{\theta}^{\perp}) \mathrm{e}^{\mu t} dt \\ &= \int_{-\sqrt{r_0^2 - s^2}}^{\sqrt{r_0^2 - s^2}} \mathrm{e}^{\mu t} dt \\ &= \frac{\mathrm{e}^{\mu\sqrt{r_0^2 - s^2}} - \mathrm{e}^{-\mu\sqrt{r_0^2 - s^2}}}{\mu}, \qquad -r_0 \le s \le r_0. \end{aligned} \tag{67}$$

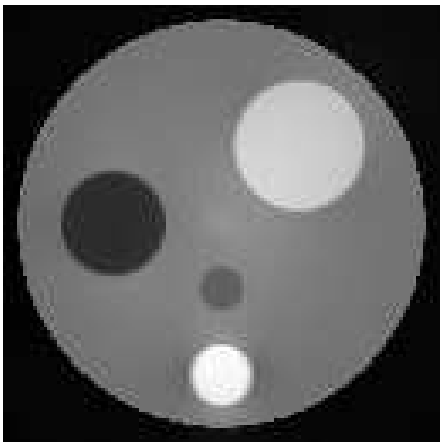

FIGURE 4. Reconstruction of the phantom using Algorithm 2 with $\mu = 0.154\text{cm}^{-1}$.

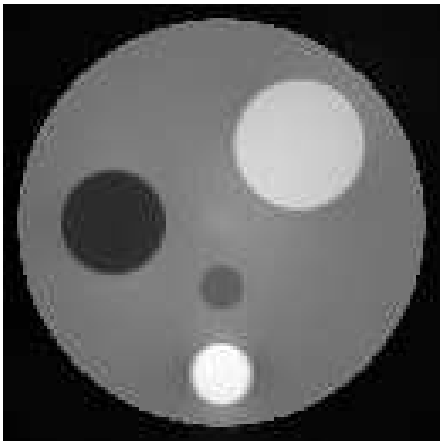

FIGURE 5. Reconstruction of the phantom using Algorithm 3 with $\mu = 0.154\text{cm}^{-1}$ and $\sigma = 10^{-}8$.

In numerical simulations, a phantom consisting of displaced disks were used (see Figure 2). The parameters of the phantom are given in Table 2. The exponential Radon transform of the phantom was analytically computed using (67), translation property

$$\begin{aligned} \mathcal{T}_\mu f_{x-y}(\boldsymbol{\theta}, s) &= \int_{\mathbb{R}^2} f(\boldsymbol{x}-\boldsymbol{y})\delta(\boldsymbol{x}\cdot\boldsymbol{\theta}-s)\mathrm{e}^{\mu\boldsymbol{x}\cdot\boldsymbol{\theta}^\perp}\,d\boldsymbol{x} \\ &= \mathcal{T}_\mu f(\boldsymbol{\theta}, s-\boldsymbol{y}\cdot\boldsymbol{\theta})\mathrm{e}^{\mu\boldsymbol{y}\cdot\boldsymbol{\theta}^\perp}, \end{aligned} \tag{68}$$

and linearity

$$\mathcal{T}_\mu[f_1+f_2](\boldsymbol{\theta}, s) = \mathcal{T}_\mu f_1(\boldsymbol{\theta}, s) + \mathcal{T}_\mu f_2(\boldsymbol{\theta}, s) \tag{69}$$

of the exponential Radon transform.

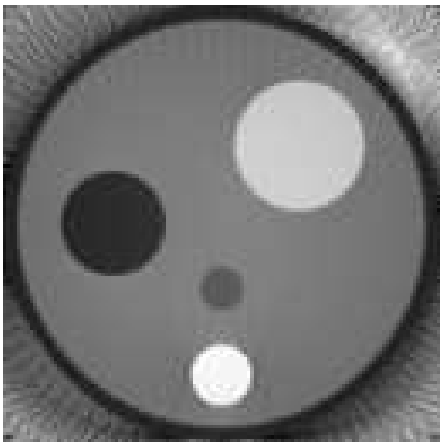

FIGURE 6. Reconstruction of the phantom using FBP of [3].

Disk #	f	r_0	c_0
1	1	6.157	$(0, 0)$
2	-1	1.572	$(-3.275, 0)$
3	1	1.965	$(2.358, 2.358)$
4	1.5	0.917	$(0, -4.5850)$
5	-0.5	0.05	$(0, -1.965)$

TABLE 2. Phantom Parameters. The phantom is made up by linear transposition of disks with attenuation f, radius r_0 and center located at c_0.

5.3.2. *Numerical Inversion.* Numerical simulations were performed on the two-dimensional phantom image corresponding to a region of $13.1 \times 13.1\text{cm}^2$, discretized by 129×129 pixels. The projections were taken from 129 equally spaces angles over 2π, and 129 parallel lines for each angle. To avoid aliasing, the image and the projections were zero-padded to 257 pixels in horizontal and vertical, and radial directions, respectively.

The $M(2)$-Fourier transform was numerically implemented as described in [9, 18, 20]. All numerical implementations were performed using MATLAB. Figures 3 to 5 show the reconstructed images using the proposed algorithms for $\mu = 0.154\text{cm}^{-1}$. The proposed algorithms are also applicable when μ is zero or purely imaginary [18, 19, 20, 21, 22].

Figure 3 shows the reconstructed image using Algorithm 1 for $\mu = 0.154\text{cm}^{-1}$ and $n = 0$. We also performed reconstructions using Algorithm 1 for $n = 1, 2, 3$. The results showed that the choice of n effects the quality of the reconstructed images. We observed that for even n values, the reconstructed images have primarily low frequency content, whereas for odd n values they have high frequency content. This observation is in agreement with the analysis provided in Section 5.2 which is summarized in Figure 1.

Figure 4 shows the reconstructed image using Algorithm 2 for $\mu = 0.154\text{cm}^{-1}$ and $n \in \{-64, \ldots 64\}$. The reconstructed image shows improvement upon Algorithm 1. We observed that although even valued n components are sufficient, using odd

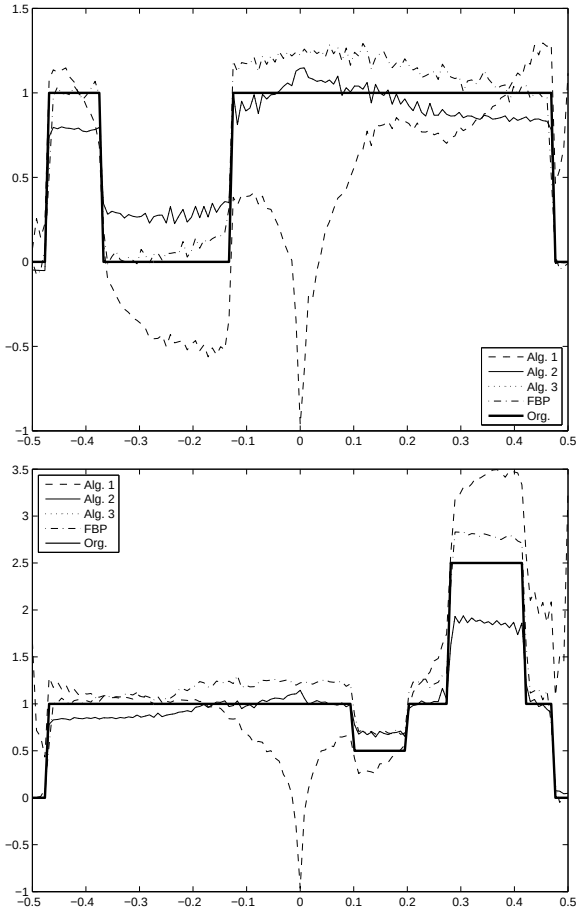

FIGURE 7. Plots of the central horizontal (top) and vertical (bottom) slices of the phantom and reconstructed images using Algorithms 1-3 and FBP.

valued n components provide better high frequency content in reconstructed images as shown by the analysis in Section 5.2 and Figure 1.

Finally, Figure 5 shows the reconstructed image using Algorithm 3 for $\mu = 0.154\text{cm}^{-1}$ and $n \in \{-64, \ldots, 64\}$. There is no noticeable difference between Algorithm 2 and Algorithm 3. However, Algorithm 2 is computationally less intensive than Algorithm 3.

Our simulations show that the reconstructed images become sharper as Fourier components with higher $|n|$ values are incorporated into the reconstruction, since these components contribute contribute to the higher frequencies of the phantom.

The numerical simulations demonstrate the applicability and the performance of the inversion algorithms. For comparison, the filtered backprojection (FBP) reconstruction [3] is shown in Figure 6. Figure 7 shows the central horizontal and vertical slices of the reconstructed phantoms using Algorithms 1, 2, 3, and FBP. Figures 4, 5, 6 and 7 show that the reconstructions obtained by Algorithms 2 and 3

are comparable to that of FBP. Note that further improvements in reconstruction is possible by improving the numerical implementation of the $M(2)$-Fourier transform.

6. Conclusion

In this paper, we presented a new approach for the inversion of the exponential Radon transform based on the harmonic analysis of the Euclidean motion group. We modified of the exponential Radon transform to obtain a convolution representation over the Euclidean motion group. Then, the convolution representation of the modified exponential Radon transform is block diagonalized in the $M(2)$-Fourier domain, leading to three new reconstruction algorithms. We discussed numerical implementation of the algorithms and their performance in simulations. The proposed convolution representation can be generalized to angle-dependent and half-scan exponential Radon transforms as well as other integral transforms of transmission and emission tomography.

Appendix A. Fourier transform over groups

Fourier analysis on groups is closely related to the theory of group representations. A unitary representation of a locally compact group G is a homomorphism U from G into the group $\mathbf{A}(H_U)$ of unitary operators on some nonzero Hilbert space H_U, i.e.

$$U : G \longrightarrow \mathbf{A}(H_U) \tag{70}$$

$$U(g_1 g_2) = U(g_1)U(g_2), \quad g_1, g_2 \in G, \tag{71}$$

and $U(g)$, $g \in G$ is a unitary operator on some Hilbert space H_U. If U is invariant on a nontrivial subspace M of H_U, i.e. $U(g)M \subset M$ for all $g \in G$, then U is called reducible, otherwise U is irreducible. For example, for each $\lambda \in \mathbb{R}$,

$$U^{(\lambda)}(x) = \mathrm{e}^{2\pi \mathrm{i}\lambda x}, \qquad x \in \mathbb{R} \tag{72}$$

acting by scalar multiplication on $H_U = \mathbb{C}$, is a irreducible unitary representation of the additive group $(\mathbb{R}, +)$. [1]

The Fourier transform $\mathcal{F}_G(f)(U)$ of a function $f \in L^1(G, d(g))$, where G is a locally compact group of Type I and $d(g)$ is the left Haar measure on G, associated with a unitary representation U of G is defined as a bounded operator on H_U. More specifically,

$$\mathcal{F}_G(f)(U) = \int_G f(g)U(g^{-1})d(g), \tag{73}$$

where the operator-valued integral is interpreted as

$$\langle \mathcal{F}_G(f)(U)u, v\rangle = \int_G f(g)\langle U(g^{-1})u, v\rangle dg, \qquad \text{for all } u, v \in H_U. \tag{74}$$

Under this definition, the Fourier transform of $f(x) \in L^1(\mathbb{R})$ associated with the representation defined in (72) is given by

$$\mathcal{F}_{\mathbb{R}}(f)(U_\omega) = \int_{\mathbb{R}} f(x)\mathrm{e}^{-2\pi \mathrm{i}\omega x} dx, \qquad \forall x \in \mathbb{R}, \tag{75}$$

which is the same as the classical Fourier transform on $\mathbb{R}$.

[1] For locally compact groups, if any unitary representation can be decomposed uniquely into a direct integral of irreducible unitary representations, the group is said to be Type I [12].

For a locally compact group G with left Haar measure $d(g)$, the convolution of $f_1, f_2 \in L^1(G, d(g))$ is defined as

$$(f_1 *_G f_2)(g) = \int_G f_1(h) f_2(h^{-1}g) d(h), \quad g \in G. \tag{76}$$

An important property of the Fourier transforms over groups is that the group convolution becomes operator composition in the Fourier space. More specifically,

$$\mathcal{F}_G(f_1 *_G f_2)(U) = \mathcal{F}_G(f_1)(U)\ \mathcal{F}_G(f_2)(U). \tag{77}$$

For two unitary representations U_1, U_2 of G, if there exists a unitary operator $V : H_{U_1} \longrightarrow H_{U_2}$, such that $U_2 = VU_1V^{-1}$ for all $x \in G$, then U_1 and U_2 are called equivalent representations. The collection of all nonequivalent irreducible representation classes of G is denoted by $\hat{G}$ and is called the dual of group G. The collection of Fourier transforms $\{\mathcal{F}(f)(\lambda)\}$ for all $\lambda \in \hat{G}$ is called the spectrum of the function f. For a separable locally compact group of Type I, the Fourier synthesis formula exists. More specifically, for uni-modular G,

$$f(g) = \int_{\hat{G}} \text{Trace}\left(U^{(\lambda)}(g)\ \mathcal{F}_G(f)(U^{(\lambda)})\right) d\nu(\lambda), \tag{78}$$

where $d\nu(\lambda)$ is the Plancherel measure of the dual group $\widehat{G}$.

Appendix B. $M(2)$-Fourier transform of distributions

Let $\mathcal{D}(M(2))$ and $\mathcal{S}(M(2))$ denote the space of compactly supported smooth and rapidly decreasing functions over $M(2)$, respectively. The dual $\mathcal{D}'(M(2))$ and $\mathcal{S}'(M(2))$ of $\mathcal{D}(M(2))$ and $\mathcal{S}(M(2))$ is called the space of distributions and tempered distributions on $M(2)$, respectively. Let $v \in \mathcal{S}'(M(2))$ be a tempered distribution. For $\varphi \in \mathcal{S}(M(2))$, the value of $v(\varphi)$ is denoted by $\langle v, \varphi \rangle$ or $\int_{M(2)} v(g)\varphi(g)d(g)$. Then the $M(2)$-Fourier transform $\widehat{v}$ of v is defined by

$$\langle \mathcal{F}_{M(2)}(v), \widehat{\varphi} \rangle = \langle \widehat{v}, \widehat{\varphi} \rangle = \langle v, \varphi \rangle. \tag{79}$$

Furthermore, if v is compactly supported then $M(2)$-Fourier transform of v can be computed by its action on $u_{mn}^{(\lambda)}(g)$ [23], i.e.

$$\widehat{v}_{mn}(\lambda) = (v, u_{mn}^{(\lambda)}(g^{-1})). \tag{80}$$

Let $v_1, v_2 \in \mathcal{S}(M(2))$, one of which is compactly supported. Then the convolution $v_1 *_{M(2)} v_2$ of v_1 and v_2 is a tempered distribution defined by either of the following ways

$$\langle v_1 *_{M(N)} v_2, \varphi \rangle = \langle v_1(h), \langle v_2(g), \varphi(hg) \rangle \rangle \tag{81}$$

$$= \langle v_2(g), \langle v_1(h), \varphi(hg) \rangle \rangle. \tag{82}$$

By (79) and (80), the $M(N)$-Fourier transform of the convolution $v_1 *_{M(N)} v_2$ is given as

$$\mathcal{F}_{M(2)}(v_1 *_{M(N)} v_2)_{mn}(\lambda) = \sum_k \widehat{v_2}_{mk}(\lambda)\widehat{v_1}_{kn}(\lambda). \tag{83}$$

Appendix C. Angle dependent exponential radon transform and 180° acquisition

C.1. Angle Dependent Exponential Radon Transform. Our approach for the exponential Radon transform inversion can be extended for the angle dependent exponential Radon transform defined by

$$\mathcal{T}_{\mu(\boldsymbol{\theta})} f(\boldsymbol{\theta}, t) = \int_{\mathbb{R}^2} f(\boldsymbol{x}) \delta(\boldsymbol{x} \cdot \boldsymbol{\theta} - t) \mathrm{e}^{\mu(\boldsymbol{\theta})\, \boldsymbol{x} \cdot \boldsymbol{\theta}^{\perp}} d\boldsymbol{x}, \tag{84}$$

where $\mu(\theta)$ is the angle dependent attenuation, $t \in \mathbb{R}$, $\boldsymbol{\theta} = (\cos\theta, \sin\theta)^T$ is a unit vector on S^1 with $\theta \in [0, 2\pi)$, and $\boldsymbol{\theta}^{\perp} = (-\sin\theta, \cos\theta)^T$. Similar to the uniform attenuation case, define the *modified angle dependent exponential Radon transform* $\mathcal{T}'_{\mu} f(g)$ as follows:

$$\mathcal{T}'_{\mu} f(R_\theta, r_1, r_2) = \mathcal{T}_{\mu(\boldsymbol{\vartheta})} f(\boldsymbol{\vartheta}, -r_1) \mathrm{e}^{\mu(\boldsymbol{\vartheta}) r_2}, \qquad \boldsymbol{\vartheta} = (\cos\theta, -\sin\theta)^T,\ r_1, r_2 \in \mathbb{R}. \tag{85}$$

Then the modified angle dependent exponential Radon transform can be expressed as a convolution operation over $M(2)$:

$$\begin{aligned}
\mathcal{T}'_{\mu} f(g) &= \mathcal{T}_{\mu(\boldsymbol{\vartheta})} f(\boldsymbol{\vartheta}, -r_1) \mathrm{e}^{\mu(\boldsymbol{\vartheta}) r_2} \\
&= \int_{\mathbb{R}^2} f(\boldsymbol{x}) \delta(\boldsymbol{x} \cdot \boldsymbol{\vartheta} + r_1) \mathrm{e}^{\mu(\boldsymbol{\vartheta})\, \boldsymbol{x} \cdot \boldsymbol{\vartheta}^{\perp} + \mu(\boldsymbol{\vartheta}) r_2} d\boldsymbol{x} \\
&= \int_{\mathbb{R}^2} f(\boldsymbol{x}) \delta(R_\theta \boldsymbol{x} \cdot \boldsymbol{e_1} + r_1) \mathrm{e}^{\mu(\boldsymbol{\vartheta})\, R_\theta \boldsymbol{x} \cdot \boldsymbol{e_2} + \mu(\boldsymbol{\vartheta}) r_2} d\boldsymbol{x} \\
&= \int_{\mathbb{R}^2} f(\boldsymbol{x}) \delta((R_\theta \boldsymbol{x} + \boldsymbol{r}) \cdot \boldsymbol{e_1}) \mathrm{e}^{\mu(\boldsymbol{\vartheta})\, (R_\theta \boldsymbol{x} + \boldsymbol{r}) \cdot \boldsymbol{e_2}} d\boldsymbol{x} \\
&= \frac{1}{2\pi} \int_0^{2\pi} \int_{\mathbb{R}^2} f(\boldsymbol{x}) \delta(\phi) \delta((R_\theta \boldsymbol{x} + \boldsymbol{r}) \cdot \boldsymbol{e_1}) \mathrm{e}^{\mu((R_\theta R_\phi)^T \boldsymbol{e_1})\, (R_\theta \boldsymbol{x} + \boldsymbol{r}) \cdot \boldsymbol{e_2}} d\boldsymbol{x} d\phi \\
&= \int_{M(2)} f_\delta(h) \Lambda(gh) d(h) \\
&= (\Lambda *_{M(2)} f^*_\delta)(g), \quad g = (R_\theta, \boldsymbol{r}) \in M(2),
\end{aligned} \tag{86}$$

where f_δ is given by

$$f_\delta(h) = f(\boldsymbol{x}) \delta(\phi), \quad h = (R_\phi, \boldsymbol{x}) \in M(2), \tag{87}$$

and Λ is the convolution filter which is given by

$$\Lambda(h) = \delta(\boldsymbol{x} \cdot \boldsymbol{e_1}) \mathrm{e}^{\mu(R_\phi^T \boldsymbol{e_1})\, \boldsymbol{x} \cdot \boldsymbol{e_2}} = \delta(\boldsymbol{x} \cdot \boldsymbol{e_1}) \mathrm{e}^{\mu(-\phi)\, \boldsymbol{x} \cdot \boldsymbol{e_2}}, \quad h = (R_\phi, \boldsymbol{x}) \in M(2). \tag{88}$$

Note that, we use the short hand notation $\mu(\phi)$ for $\mu(R_\phi \boldsymbol{e_1})$.

Treating the projections and the convolution filter as tempered distributions (See Appendix B), the modified angle dependent exponential Radon transform can be expressed as a multiplication in the $M(2)$-Fourier transform domain, which can be inverted using (31).

C.2. Exponential Radon Transform for the Half-Scan Problem. Determination of f given $\mathcal{T}_\mu f(\boldsymbol{\theta}, t)$ for $\theta \in [0, \pi)$ for fixed $\mu \in \mathbb{C}$ is known as the half-scan problem, i.e. reconstruction from 180° acquisition [24, 25, 26]. The half-scan problem can be expressed as a deconvolution problem over $M(2)$. To do so, we extend

the projections by using the reflection property of the exponential Radon transform as shown in [24, 25]. Let

$$\mathcal{T}_{180^\circ} f(\boldsymbol{\theta}, t) = \begin{cases} \mathcal{T}_\mu f(\boldsymbol{\theta}, t), & \theta \in [0, \pi) \\ \mathcal{T}_\mu f(-\boldsymbol{\theta}, -t), & \theta \in [\pi, 2\pi) \end{cases} . \tag{89}$$

Since exponential Radon transform satisfies the identity

$$\mathcal{T}_\mu f(\boldsymbol{\theta}, t) = \mathcal{T}_{-\mu} f(-\boldsymbol{\theta}, -t), \tag{90}$$

$\mathcal{T}_{180^\circ} f$ can be expressed as the angle dependent exponential Radon transform of f

$$\mathcal{T}_{180^\circ} f(\boldsymbol{\theta}, t) = \mathcal{T}_{\mu(\boldsymbol{\theta})} f(\boldsymbol{\theta}, t), \tag{91}$$

where

$$\mu(\theta) = \begin{cases} \mu, & \theta \in [0, \pi) \\ -\mu, & \theta \in [\pi, 2\pi) \end{cases} . \tag{92}$$

Acknowledgements

We would like to thank to Dr. Joyce McLaughlin and Dr. David Isaacson for their invaluable discussions. This work was partially supported by National Science Foundation under grant NSF-BES-0363160.

References

[1] F. Natterer, "The Mathematics of Computerized Tomography," New York, NY: Wiley-Teubner, 1986.
[2] A. Puro, *Cormack-type inversion of exponential Radon transform*, Inverse Problems, **17** (2001), 179–188.
[3] O. Tretiak and C. Metz, *The exponential radon transform*, SIAM J. Appl. Math., **39** (1980), 341–354.
[4] G. W. Hawkins, P. K. Leichner, and N.-C. Yang, *The circular harmonic transform for SPECT reconstruction and boundary conditions on the fourier transform on the sinogram*, IEEE Transactions on Medical Imaging, **7** (1988), 135–148.
[5] C. Metz and X. Pan, *A unified analysis of exact methods of inverting the 2-d exponential Radon transform, with implications for noise control in spect*, IEEE Transactions on Medical Imaging, **14** (1995), 643–658.
[6] P. Kuchment and I. Shneiberg, *Some inversion formulas in the single photon emission computed tomography*, Applicable Analysis, **53** (1994), 221–231.
[7] S. Bellini, M. Piancentini, C. Cafforio, and F. Rocca, *Compensation of tissue absorption in emission tomography*, IEEE Transactions on Acoustics, Speech and Signal Processing, **ASSP-27** (1979), 213–218.
[8] T. Inouye, K. Kose, and A. Hasegawa, *Image reconstruction algorithm for single-photon-emission computed tomography with uniform attenuation*, Phys. Med. Biol., **34** (1989), 299–304.
[9] A. Kyatkin and G. Chirikjian, *Algorithms for fast convolutions on motion groups*, Applied Computational Harmonic Analysis, **9** (2000), 220–241.
[10] B. Yazıcı, *Stochastic deconvolution over groups*, IEEE Transactions in Information Theory, **50** (2004), 494–510.
[11] M. Sugiura, "Unitary Representations and Harmonic Analysis," Tokyo: Kodansha, 1975.
[12] N. J. Vilenkin, "Special Functions and the Theory of Representations," Providence, RI: American Mathematical Society, 1988.
[13] R. T. Seeley, *Spherical harmonics*, The American Mathematical Monthly, **73** (1966), 115–121.
[14] C. W. Groetsch, "Generalized Inverses of Linear Operators : Representation and Approximation," New York, NY: M. Dekker, 1977.
[15] A. N. Tikhonov, V. Arsenin, and F. John, "Solutions of Ill-Posed Problems," Washinton, D.C.: V. H. Winston & Sons, 1977.

[16] F. Natterer and F. Wübbeling, "Mathematical Methods in Image Reconstruction," Philadelphia, PA: SIAM, 2001.
[17] I. M. Gelfand and G. E. Shilov, "Generalized Functions, Properties and Operations," Vol. 1, New York, NY: Academic Press, 1964.
[18] C. E. Yarman and B. Yazıcı, *Radon transform inversion via wiener filtering over the Euclidean motion group*, in "Proceedings of IEEE international Conference on Image Processing 2003," 2, Barcelona, Spain, 2003, 811–814.
[19] ——, *Radon transform inversion based on harmonic analysis of the Euclidean motion group*, in "Proceedings of IEEE International Conference on on Acoustics, Speech, and Signal Processing 2005," 2005.
[20] ——, *Exponential Radon transform inversion based on harmonic analysis of the Euclidean motion group*, in "Proceedings of IEEE International Conference on Image Processing 2005," 2005.
[21] B. Yazıcı and C. E. Yarman, *Deconvolution over groups in image reconstruction*, in "Advances in Imaging and Electron Physics," San Diego, CA: Academic Press, 2006, vol. 141, 257–300.
[22] C. E. Yarman and B. Yazıcı , *An inversion method for the exponential Radon transform based on harmonic analysis of the Euclidean motion group*, in "Proceedings of SPIE Medical Imaging 2006," San Diego, CA, 2006.
[23] G. Warner, "Harmonic Analysis on Semi-Simple Lie Groups I," Berlin, Germany: Springer-Verlag, 1972.
[24] F. Noo and J.-M. Wagner, *Image reconstruction in* $2D$ *SPECT with* 180° *acquisition*, Inverse Problems, **17** (2001), 1357–1371.
[25] X. Pan, C.-M. Kao, and C. Metz, *A family of* π*-scheme exponential Radon transforms and the uniqueness of their inverses*, Inverse Problems, **18** (2002), 825–836.
[26] H. Rullgård, *An explicit inversion formula for the exponential Radon transform using data from* 180°, Arkiv för Matematik, **42** (2004), 353–362.

Received for publication December 2006.

E-mail address: yarman@ecse.rpi.edu
E-mail address: yazici@ecse.rpi.edu